IEEE Access
Multidisciplinary ⋮ Rapid Review ⋮ Open Access Journal

Received April 7, 2021, accepted April 18, 2021, date of publication April 27, 2021, date of current version May 6, 2021.

Digital Object Identifier 10.1109/ACCESS.2021.3075935

Regenerative Active Electronic Load With Current, Voltage and Frequency Control for Power Transformer Testing

GUILHERME MONTEIRO DE REZENDE[1,2], MATHEUS VIEIRA DE ALMEIDA[3], TIAGO DE SÁ FERREIRA[1,2], (Member, IEEE), CLODUALDO VENICIO DE SOUSA[1], AND VICTOR FLORES MENDES[2,3], (Member, IEEE)

[1]Instituto de Ciências Tecnológicas, Universidade Federal de Itajubá, Itabira Campus, Itabira 37500-903, Brazil
[2]Graduate Program in Electrical Engineering, Universidade Federal de Minas Gerais, Belo Horizonte 31270-901, Brazil
[3]Department of Electrical Engineering, Universidade Federal de Minas Gerais, Belo Horizonte 31270-901, Brazil

Corresponding author: Guilherme Monteiro de Rezende (guilhermemre@unifei.edu.br)

This work was supported in part by the Universidade Federal de Itajubá (UNIFEI), and in part by the Brazilian Agencies: the Fundação de Amparo à Pesquisa de Minas Gerais (FAPEMIG), the Coordenação de Aperfeiçoamento de Nível Superior (CAPES), and the Conselho Nacional de Desenvolvimento Científico e Tecnológico (CNPq).

ABSTRACT The long duration test of electrical equipment is an important tool for users and manufacturers to determine precise information as, for example, equipment operational limits, lifespan, thermal behavior, etc. Although useful, these long duration tests are usually conducted using passive elements such as in the burn-in test, consuming a great amount of energy and with limited flexibility to emulate different loading profiles (e.g., current and voltage levels, harmonics content, etc.). In this context, to perform tests in power transformer emulating its real operation conditions can be a difficult task, since the standards procedures do not emulate the loading levels and the burn-in test consumes a high quantity of energy. Moreover, in distribution networks, the transformers are submitted to an increasing level of nonlinear voltage and current. Thus, it is important to test them under these conditions. The use of active electronic loads (AEL) is an alternative to solve these problems since the device structure can have regenerative proprieties and its control can emulate different types of load. This paper presents an AEL to perform tests in power transformers with low energy consumption that is capable of imposing controlled voltage and current (frequency, level, and harmonic distortion) to the transformer under test. The proposed methodology is validated by experimental results of a 50 kVA prototype.

INDEX TERMS Active electronic load, load emulator, power transformer test, resonant control, voltage and frequency control.

I. INTRODUCTION

Driven mainly by the development of the economies of emerging countries, the world's electrical energy demand has not only risen in recent decades, but also maintains an expected upward trend until at least 2040 [1]. This trend is also accompanied by a growing concern about the environmental impacts caused by traditional thermal-based generation, changing the nations mindset towards a more sustainable energy matrix and rational energy consumption [2].

Long duration tests of electrical equipment are an essential step in the design and conception of devices, as it allows both the user and the manufacturer to establish the operational characteristics of the equipment, as predicting its thermal behavior and lifespan, defining its maintenance plan, estimating its parameters, anticipating possible failures, stipulating permissible loads, among others. However, traditional tests are widely accomplished by employing passive loads that consume a considerable amount of energy throughout the whole process without necessarily producing useful work.

From a technical point of view, in addition to the high energy consumption of long-term tests, another complicating factor is often the need for the emulation of non-linear loads and/or grid power quality disturbances. With the widespread use of electronic devices, there is a significant presence of harmonic currents as well as distortions in the voltage

The associate editor coordinating the review of this manuscript and approving it for publication was Sanjeevikumar Padmanaban.

waveform of the power lines to which these equipment are connected [3]. Therefore, it is important for the equipment be tested in the closest conditions to those in which they will be used, which includes being under the effect of such distortions, allowing, for example, accurate efficiency measurement and lifetime analysis.

In this context of more rational and sustainable use of electric energy and the need to perform tests on equipment with non-linear behavior content, active electronic loads (AEL), also referred to as dynamic electronic load simulators (DELS), are an appealing solution [4]. These AELs are equipment based on static converters capable of emulating load profiles with great flexibility in terms of amplitudes and frequencies of their synthetized output waves. As an added benefit, they can also have energy regeneration capabilities when built with back-to-back converters. This class of AEL devices can be used for a variety of purposes such as testing devices for power systems protection [4], uninterruptible power supplies (UPS) [5], electronic ballasts [6], and inverters [7], as well as emulating different sources and/or loads of microgrids [8], solar panels [9], [10], and AC circuits in general [11], [12].

The application of AELs are specially of great interest in routine tests on power transformers [13]–[15]. In the particular study of transformers, some typical indirect tests such as short-circuit and open circuit [16] neglect, at some level, the equipment's real behavior, since it is not tested simultaneously as a whole (both current-wise and voltage-wise) under rated conditions [17]. Other common tests that employ full passive loads are not flexible and, as already mentioned, imply in high energy consumption. In contrast, the AEL presented in [18], for example, shows that the topology allows the regeneration of a large portion of the energy involved in the test back to the mains network while still allowing the control of the loading levels and current harmonic distortion flowing though the studied equipment.

The increase of electronic devices and distributed generation (DG) connected to the grid changed both its and the power transformers operation, and some problems, such as overvoltage and voltage distortion became more common [19], [20]. Therefore, it is very important to test transformers under distorted voltage and current conditions. None of the AEL's presented in [13]–[15], [18] are able to emulate these operational conditions, since they do not have voltage and frequency control capabilities.

This paper presents an AEL topology for testing power transformers that can emulate these non-ideal conditions and also recovers part of the energy used in the test to the grid. The system presents the flowing control features: voltage and current level, voltage and current harmonic distortion, frequency, and power factor. Furthermore, the proposed AEL can be used to test other devices that allows energy flow through them, such as general power inverters, UPS, and circuit breakers. This structure with a high degree of freedom of control distinguishes itself from others presented in literature and is, therefore, the main contribution of this work.

The paper is organized as follows: in section II, the proposed AEL's working principle and its control strategy are explained, which includes the mathematical modeling, control structures, controllers design, and stability analysis. Section III presents and discusses all experimental results, validating the capabilities of the proposed system. Lastly, the final conclusions of this paper are presented in Section IV.

II. AEL SYSTEM DESCRIPTION

First, a brief description of the operating principle is provided, and then, the control strategies necessary for carrying out the transformer test are discussed.

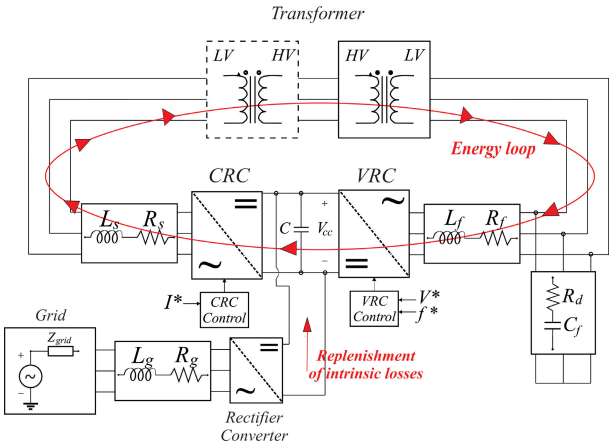

FIGURE 1. Transformer test bench schematic.

A. WORKING PRINCIPLE

In Fig. 1, a simplified schematic of the power transformer test setup is provided. The proposed system consists of three converters that share the same dc bus: the rectifier converter (RC), connected to the electrical network through an L filter, the voltage regulator converter (VRC), and the current regulator converter (CRC). The two latter operate isolated from the power system and are connected to the transformer under test by two filters: the VRC, by a passively (resistance) damped LC filter, and the CRC, by an L filter. The filters are shown in Fig.1 and the resistances of the inductances are explicitly represented. These converters are the focus of this paper, since they are responsible for controlling the test variables (current and voltage).

The VRC acts imposing a controlled voltage on the filter capacitor and, consequently, on the transformer under test. As there is no connection to the power grid, the imposed voltage level and frequency are controlled by the VRC. In addition, with harmonic control, the VRC can also synthetize multiple low-order voltage harmonics submitting the transformer to a controlled distortion. The CRC acts controlling the current flowing thorough the L filter and, hence, the transformer current. The CRC can also impose the current level, and harmonic distortion, fully controlling the transformer loading profile in combination with VRC.

As depicted in Fig. 1, the VRC and CRC operation establishes an energy loop. The test current imposed by the CRC

has two possible paths: to flow to the LC filter capacitor or to the VRC. As the VRC controls the LC capacitor voltage to a constant operation point, the current level in this branch is also constant to maintain test voltage level. Thus, the test current has no other way than return to the dc bus though VRC, recharging it. This energy recovery allows the proposed test bench to perform high power long duration tests with low energy consumption. The test voltage can be changed, but the variation is much slower than the current variation, thus, the energy recovery is globally kept.

The RC purpose is to supply the energy to the system, maintaining the dc bus voltage level and enabling the operation of both VRC and CRC. Since the VRC regenerates a considerable portion of the energy used in the test to the dc bus, the RC supplies only the intrinsic losses of the test bench, such as converter, filter, and transformer losses.

Finally, the equipment under test can be a single or two transformers with their high voltage windings connected, as depicted in Fig.1. This latter configuration allows the test of medium voltage transformers while connected to low voltage grid (e.g., two distribution transformers of 13.8 kV/220 V) and without the necessity of medium voltage converters. Thus, since the operational conditions of both transformers are similar, they can be tested simultaneously.

B. MATHEMATICAL MODEL

Despite controlling different test variables, the VRC and CRC controls interfere with each other's operation. A multivariable mathematical approach to the problem could lead to complex control laws and it is not used in this work. Instead, the mathematical models used to obtain the control laws of each converter are derived from the principle that each converter's controlled variable acts as a disturbance to the other. Furthermore, as the voltage is changed much slower than the current, this simplified approach allows each converter control law to be determined individually. The system control is performed in the stationary frame ($\alpha\beta$ frame), so the following equations are presented using space vector quantities.

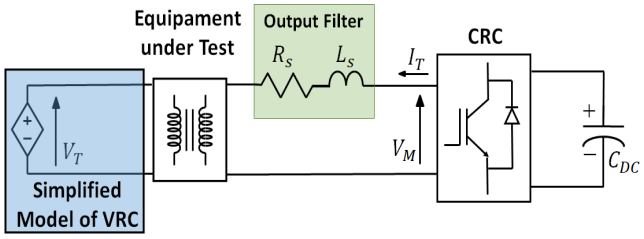

FIGURE 2. CRC + filter equivalent single-phase circuit.

Fig. 2 shows the CRC connection schematic with the VRC simplified to a controlled voltage source treated as disturbance to the control system. Equation (1) describes the dynamic behavior of the CRC current.

$$V_{M\alpha\beta} = (R_s + R_e)\, I_{T\alpha\beta} + (L_s + L_e)\, \frac{dI_{T\alpha\beta}}{dt} + V'_{T\alpha\beta} \quad (1)$$

where $V_{M\alpha\beta}$ is the voltage imposed by CRC, $I_{T\alpha\beta}$ is the transformer test current, $V'_{T\alpha\beta}$ is the reflected test voltage controlled by the VRC, R_s and L_s are the output filter resistance and inductance, and R_e and L_e are the equipment under test's equivalent resistance and equivalent inductance. The transformer magnetization inductance is neglected in the model, since its value is considerable higher than the leakage inductance.

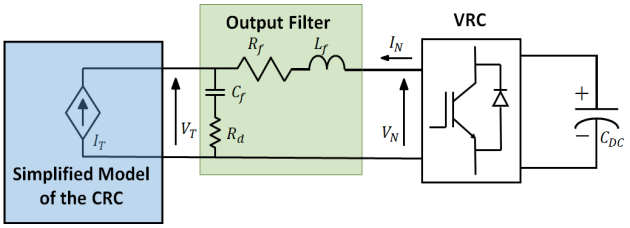

FIGURE 3. VRC + filter equivalent single-phase circuit.

Fig. 3 shows the VRC connection, with the CRC being simplified to a controlled current source. Equations (2) and (3) represent the current and voltage dynamic behavior of the LC output filter, and (4) represents the controlled test voltage.

$$V_{N\alpha\beta} = R_f I_{N\alpha\beta} + L_f \frac{dI_{N\alpha\beta}}{dt} + V_{T\alpha\beta} \quad (2)$$

$$I_{T\alpha\beta} + I_{N\alpha\beta} = C_f \frac{dV_{C\alpha\beta}}{dt} \quad (3)$$

$$V_{T\alpha\beta} = R_d \left(I_{T\alpha\beta} + I_{N\alpha\beta}\right) + V_{C\alpha\beta} \quad (4)$$

where, $V_{N\alpha\beta}$ is the voltage imposed by the VRC, $I_{N\alpha\beta}$ is the test current imposed by the VRC, $V_{C\alpha\beta}$ is the capacitor voltage, R_f and L_f are the output filter resistance and inductance, respectively, and R_d is the damping resistor.

All control laws are developed using (1) to (4), which shows the importance of the converters' output filters in the system's dynamics. Therefore, a classical design procedure was used to determine the filters components, as described in [21]–[23].

C. CONTROL STRUCTURE

The objective of the test is to synthetize voltages and currents with specific frequencies (fundamental and harmonics). One alternative is to use proportional-resonant (PR) controllers, which has become an increasingly popular alternative to the control of static converters due to their ability to present zero steady state error at a given frequency [24]–[26]. In this paper, a non-ideal PR controller is used, whose expression is presented in (5).

$$G_{PR}(s) = Kp + \sum_{h=1}^{h=6k\pm1} Kr_h \frac{2\omega_c s}{s^2 + 2\omega_c s + (h\omega_o)^2} \quad (5)$$

where h is the harmonic order of interest, ω_o is the system's fundamental frequency, Kp is the proportional gain, Kr_h is the $h\omega_o$ frequency resonant gain, and ω_c is the bandwidth around the resonant frequency. Furthermore, (5) is discretized using the Tustin rule (or trapezoidal rule) with pre-warping

and a sampling period T_s as presented in (6) for each of the frequencies of interest $h\omega_o$. This method is a common choice to implement digital PR controllers since it can correctly match the continuous resonant frequency to its discrete counterpart [27].

$$s = \frac{h\omega_o}{\tan\left(\frac{h\omega_o T_s}{2}\right)}\left(\frac{z-1}{z+1}\right) \tag{6}$$

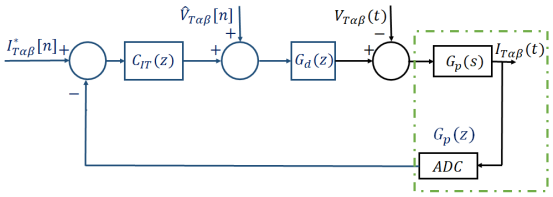

FIGURE 4. CRC control block diagram.

Fig. 4 depicts the CRC control block diagram, where $C_{IT}(z)$ is the PR controller discretized transfer function. The $G_d(z)$ block represents the delay of all computational calculations and PWM action, modeled by a unitary delay. The $G_p(s)$ is the plant continuous transfer function based on the dynamic equation presented in (1) and $G_p(z)$ it is its discrete time counterpart using zero order hold (ZOH) approximation, due to the analog to digital converter (ADC) operation. Finally, $\hat{V}_{T\alpha\beta}[n]$ represents the feedforward action of the measured test voltage $V_{T\alpha\beta}(t)$.

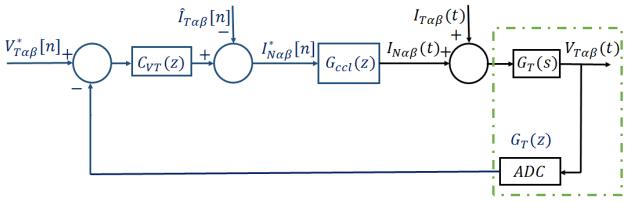

FIGURE 5. VRC control block diagram.

The VRC control, as showed in Fig.5, is implemented in a cascaded structure with an internal current loop and an external voltage loop. The structure of the VRC current loop is similar for the CRC, depicted in Fig. 4, with the transfer function $G_p(s)$ based on (2). This inner loop is represented by the $G_{ccl}(z)$ function. The continuous test voltage transfer function $G_T(s)$ is based on (3) and (4), and $G_T(z)$ is its discrete time model using ZOH approximation. The PR controller discrete transfer function is $C_{VT}(z)$, and $\hat{I}_{T\alpha\beta}[n]$ represents the feedforward action of the measured test current $I_{T\alpha\beta}(t)$.

The structures shown in Figs. 4 and 5 are implemented in the test bench. As stated, to simplify the controller design, a single output control is considered, which makes each control loop a disturbance to its counterpart. As these disturbances are the controlled quantities when performing the testing, it is expected that the feedforward actions will help mitigate the influence of each control loop on the other converter.

D. PR CONTROLLER'S GAINS CALCULATION

There is a vast literature regarding the design of PR controllers [28]–[30]. In the present work, the main objective of the control design is to conduct long duration tests controlling all electrical quantities, minimizing the control error, and rejecting disturbances.

Using frequency response analysis methods, the controller gains were determined in order to achieve stability in closed loop system and at least 30° of open loop phase-margin [31]. A sample rate of 9 kHz was used. With these criteria and based on the structure shown in Fig. 4, the gains of CRC current controller are determined in two steps.

The first one is the determination of the proportional gain (Kp). According to [32], Kp is mainly responsible for the system stability, and the resonant controllers have influence just in its vicinity. Furthermore, to ensure stability, these resonant controllers must be tuned in frequencies bellow the crossover frequency established by Kp. Thus, its value is determined so that all poles are inside the unitary circle in the z-domain and the crossover frequency is greater than a desired value. The harmonics of order $6k \pm 1$ (k is a positive integer) are the most common in power systems, so, in this work, the crossover frequency must be higher than the 7th harmonic (420 Hz), allowing the AEL to synthetize the most impactful harmonics (5^{th} and 7^{th}). With these constraints, the Kp value was select to set the crossover frequency as shown in Fig. 6.

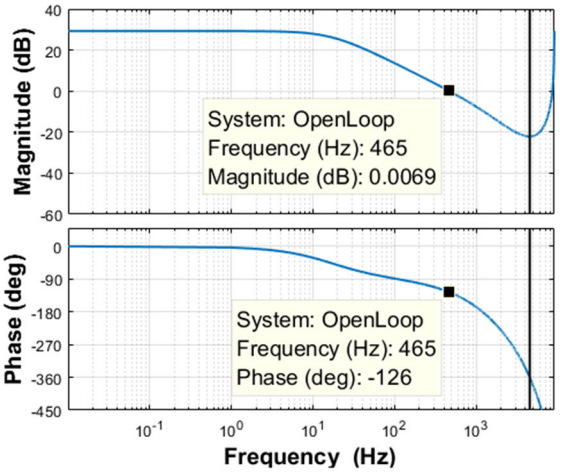

FIGURE 6. CRC current control open loop Bode plot considering only the proportional gain.

In the second step, the resonant gains are determined to meet all the design constraints. Fig. 7 presents the Bode plot of the open loop function considering all resonant controllers (60Hz, 300Hz and 420Hz). One can see from Fig. 7 that all the resonant frequencies are still below the crossover frequency and that the phase margin is 35°. Fig. 8 presents the location of all closed loop poles and zeros on the z-plane. The zoom in Fig.8 shows the poles and zeros that are close to unitary circle, because of the PR controllers. As there are no poles outside the unitary circle, the system is stable in closed loop.

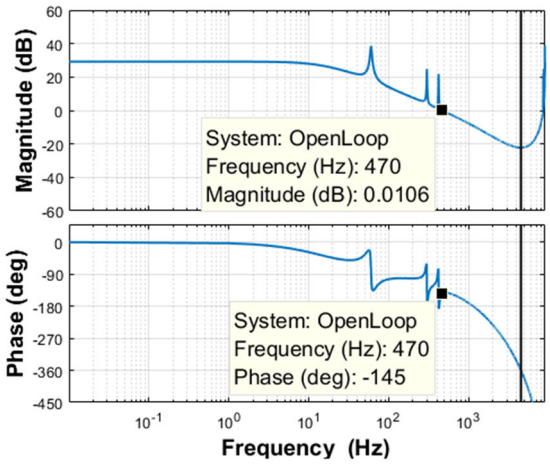

FIGURE 7. CRC current control open loop Bode plot with PR controller.

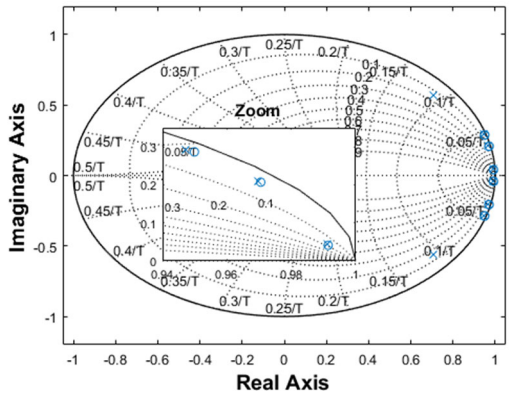

FIGURE 8. CRC closed loop poles and zeros' locations on the z-plane.

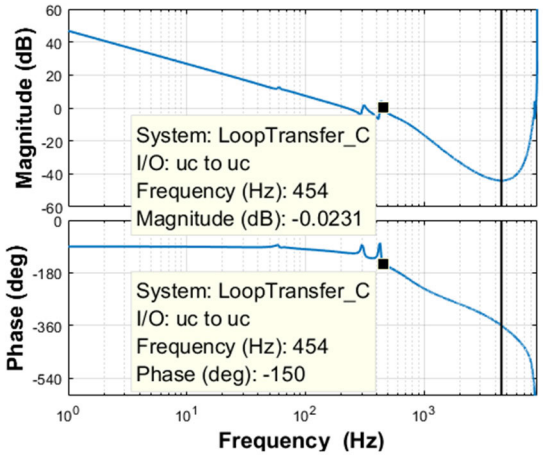

FIGURE 9. VRC voltage control open loop Bode plot with PR controller.

The same methodology was used for both the VRC current and voltage control, resulting in the Bode and z-plane map plots presented in Figs. 9 and 10. They show that VRC control has a phase margin of 30° and is stable since all poles and zeros are inside unitary circle. The designed gains are presented in Table 1.

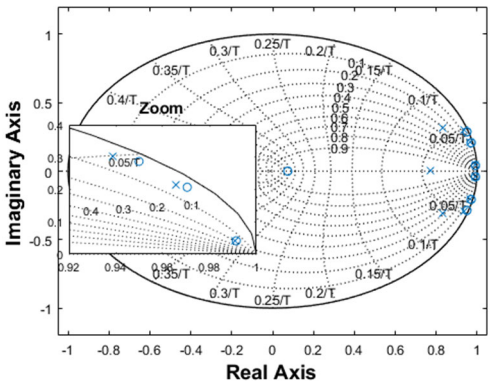

FIGURE 10. VRC closed loop poles and zeros' locations on the z-plane.

TABLE 1. PR controllers' gains.

	Kp	Kr_h
CRC current loop	6.10 Ω	61.0 F^{-1}
VRC current loop	3.01 Ω	30.1 F^{-1}
VRC voltage loop	0.11 Ω^{-1}	0.022 H^{-1}

TABLE 2. Converter's parameters.

Output Voltage (RMS)	480 V
Output current (RMS)	42 A
dc Bus Voltage	1100 V
Rated Power	50 kVA
Switching Frequency	9 kHz
Semiconductor	SEMiX653GB176HDs
Semiconductor Breakdown Voltage	1700 V

III. EXPERIMENTAL RESULTS

To validate the test structure and its control, a prototype of the proposed AEL was assembled with the parameters presented in Tables 2, 3 and 4. Fig. 11 shows the power structure formed by the power converters and their output filters, and the transformer under test. The AEL signal conditioning board and control structure are depicted in Fig. 12. Current and voltage measurements are performed using LEM HAS-50 and LEM LV25p/SP2 sensors, respectively, and the control is implemented in a DSpace 1103 platform.

The experimental results are based on the reference values presented in Table 5 that represent the phase to neutral sinusoidal peak values. The tests are divided as follows:

- Fundamental frequency test: the transformer is only submitted to fundamental voltage and current components. The transformer is submitted to 60 Hz and 30 Hz of fundamental frequency.

TABLE 3. Output filter components' values.

	CRC	VRC
Filter Inductance	1.0 mH	1.0 mH
Filter Resistance	0.01 Ω	0.01 Ω
Filter Capacitance	---	80 μF
Damping Resistance	---	1.5 Ω

TABLE 4. Transformer parameters.

Rated Power	50 kVA
Primary Winding Voltage	480 V
Secondary Winding Voltage	220 V
Winding Inductance	0.541 mH
Winding Resistance	0.09 Ω
Rated Frequency	60 Hz

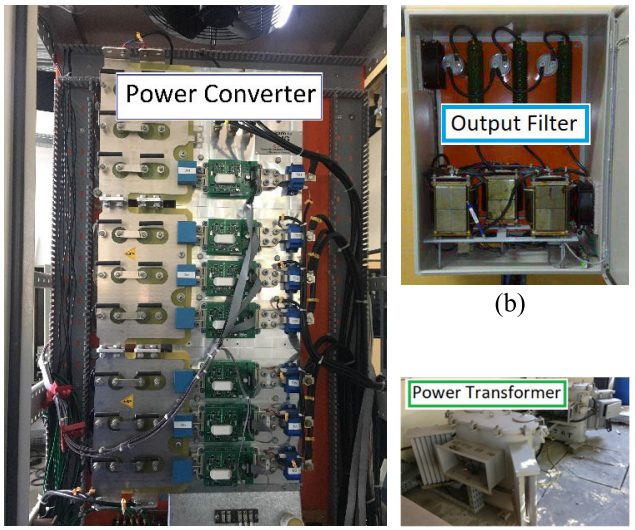

FIGURE 11. Transformer test bench power components. (a) – Static converters, (b) – Output filter and (c) – Power transformers.

- Harmonic test: The transformer is submitted to voltage and current with the fundamental frequency plus fifth and seventh harmonic components.

During the tests, the fundamental and harmonic references levels are kept constant. The system control performance results are presented first, then the real measured test quantities. To evaluate the system performance, the steady state error of the controlled variable is calculated as well as the total harmonic distortion (THD) and the individual harmonic distortion (IHD).

A. FUNDAMENTAL FREQUENCY TESTS

The transformer was submitted to fundamental voltage and current components. Fig. 13 presents the results of the voltage control loop of VRC and the current control loop of CRC, respectively, for the test at rated frequency of 60 Hz.

TABLE 5. Voltage and current references test values.

	Voltage	Current
Fundamental	180 V	15 A
5th harmonic	18 V (*IHD = 10%*)	1.5 A (*IHD = 10%*)
7th harmonic	18 V (*IHD = 10%*)	1.5 A (*IHD = 10%*)
THD	14%	14%

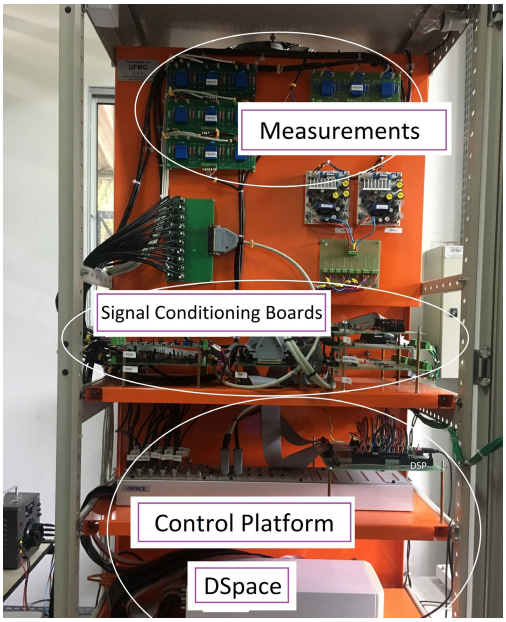

FIGURE 12. Transformer test bench measurements, signal processing and control hardware.

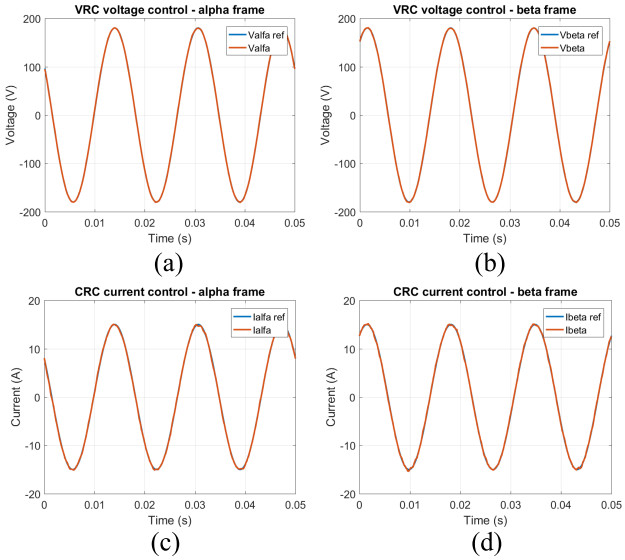

FIGURE 13. VRC and CRC voltage and current control loop reference tracking in fundamental frequency test of 60 Hz. Voltage in (a) alpha frame and (b) beta frame, Current in (c) alpha frame and (d) beta frame.

Examining Fig 13, one can see that the controller can track the sinusoidal reference. For the voltage control, error values of 0.62% and 0.66% are seen for the alpha and beta frames, respectively. For the current control, the error values are 1.42% for the alpha and 1.52% for the beta frame. The control is stable and acceptable errors smaller than 2% are obtained.

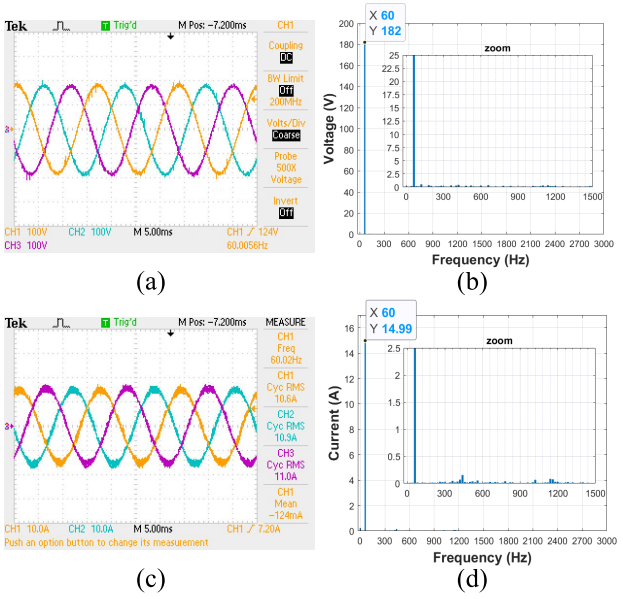

FIGURE 14. Measured fundamental frequency test results for 60 Hz. (a) Three-phase test voltage, (b) Frequency spectrum of the voltage test, (c) Three-phase test current, (d) Frequency spectrum of the current test.

Fig. 14 presents the measured three-phase voltage and current in the low voltage side of the transformer and their frequency spectrum (harmonic until the 50th order). The fundamental values are close to the reference, and a low THD (1.03% and 1.86% for voltage and current, respectively) is obtained in this test.

In order to demonstrate the AEL feasibility of testing transformers under different fundamental frequencies, the control results for 30 Hz operation are presented in Fig 15. Again, small errors are registered (for the voltage 0.85% and 1.42%, for the alpha and beta frames, and for the current 1.70% and 2.39%, for the alpha and beta frames) even if the filter is not operating under the rated conditions. Despite higher than the errors presented in the 60 Hz test, the error are still acceptable.

Lastly, Fig. 16 shows the three-phase voltage and current waveforms, and their corresponding frequency spectrums. The fundamental values are in close agreement with the reference, a with THD of 1.24% and 2.45% for voltage and current distortion, respectively.

B. HARMONIC TESTS

In the harmonic test, the transformer is submitted to distorted voltage and current. The first harmonic test applies only voltage distortion (5th and 7th harmonics) and maintains a fundamental current (60Hz) flowing through the power

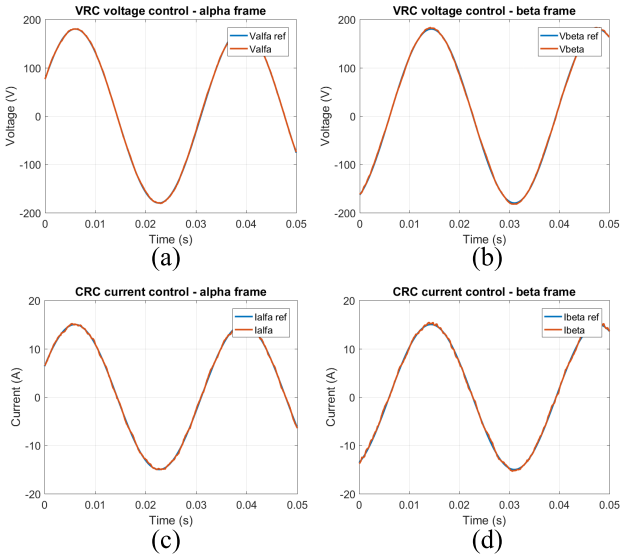

FIGURE 15. VRC and CRC voltage and current control loop reference tracking in fundamental frequency test of 30 Hz. Voltage in (a) alpha frame and (b) beta frame, Current in (c) alpha frame and (d) beta frame.

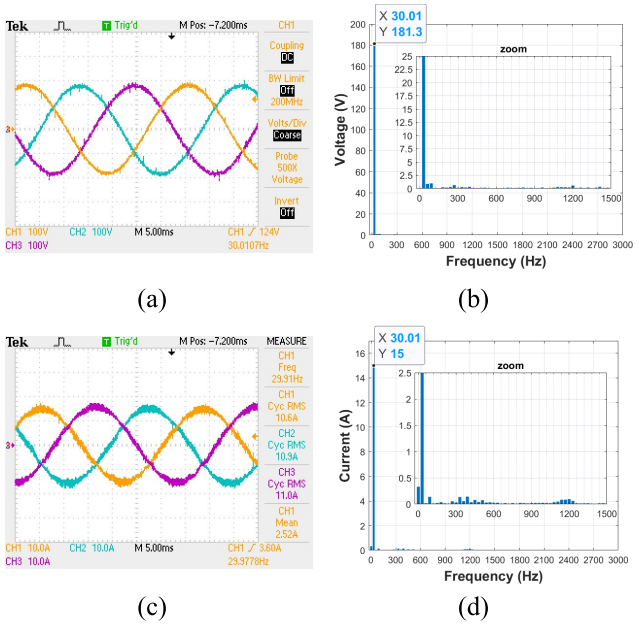

FIGURE 16. Measured fundamental frequency test results for 30 Hz. (a) Three-phase test voltage, (b) Frequency spectrum of the voltage test, (c) Three-phase test current, (d) Frequency spectrum of the current test.

transformer. Fig. 17 presents the VRC voltage loop control and CRC current loop control, and Fig. 18 presents the three-phase transformer voltage and current waveforms and their frequency spectrums.

The control variables show small tracking errors, confirmed by the frequency spectrums of the responses. Nevertheless, in the current control, a small distortion is noticed, seen as low order harmonics in Fig.18(d). It is important to highlight that a condition with voltage harmonic distortion and without current distortion is generally unreal. Therefore,

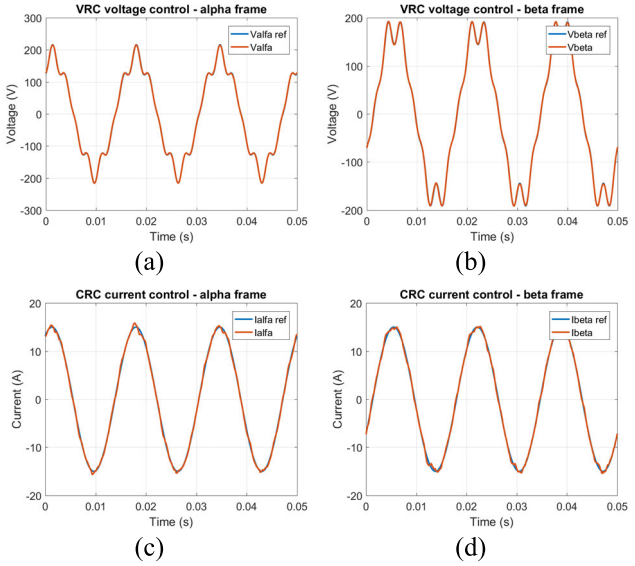

FIGURE 17. VRC and CRC voltage and current control loop reference tracking in voltage harmonic test. Voltage in (a) alpha frame and (b) beta frame, Current in (c) alpha frame and (d) beta frame.

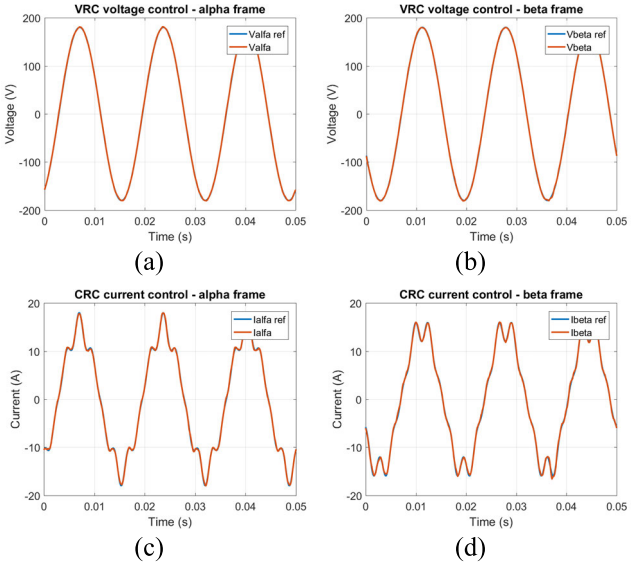

FIGURE 19. VRC and CRC voltage and current control loop reference tracking in current harmonic test. Voltage in (a) alpha frame and (b) beta frame, Current in (c) alpha frame and (d) beta frame.

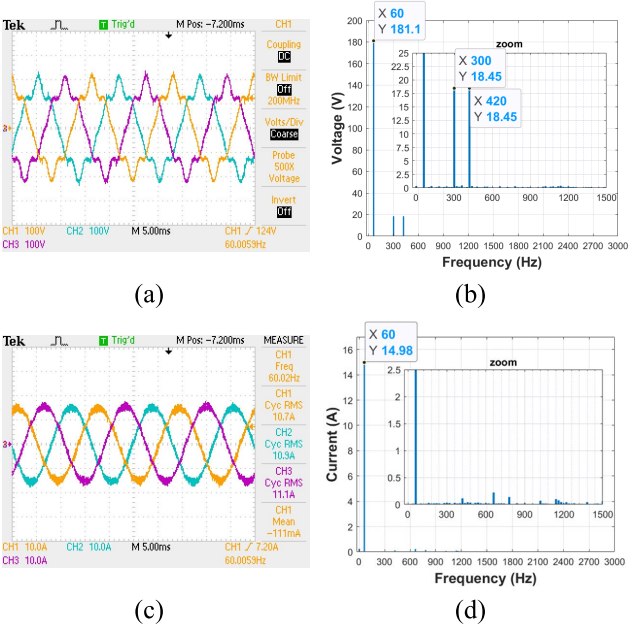

FIGURE 18. Measured voltage harmonic test results. (a) Three-phase test voltage, (b) Frequency spectrum of the voltage test, (c) Three-phase test current, (d) Frequency spectrum of the current test.

TABLE 6. Control system error for the harmonic test when the transformer is submitted separately to voltage and current distortion.

	Voltage Harmonic Test		Current Harmonic Test	
	alpha frame	beta frame	alpha frame	beta frame
Voltage loop	0.83%	0.93%	0.70%	0.79%
Current loop	2.86%	3.15%	1.51%	2.08%

TABLE 7. Voltage and current harmonic distortions in the harmonic tests.

	Voltage Test		Current Test	
	voltage	current	voltage	current
THD	14.45%	2.51%	1.32%	14.21%
IHD 5th	10.19%	0.19%	0.05%	10.07%
IHD 7th	10.19%	0.76%	0.30%	9.77%

this test demonstrates the capability of decoupled control of the converters, even if a small distortion in the current is produced.

The next test accounts for fundamental voltage and distorted current (5^{th} and 7^{th} harmonics). The results are shown in Figs. 19 and 20. In this case, the errors are also small, and the decoupled control of the converters is again demonstrated.

Analyzing Figs. 17 and 19, the designed controllers can track and/or mitigate low frequencies harmonics. This is highlighted by evaluating the controller errors presented in Table 6. Although they are greater than those presented in fundamental frequency test, the highest errors are around the 3% mark, and are not much larger than the previous results. The THD and IHD values are presented in Table 7. All values of distortion are similar to the targets presented in Table 5, showing the capability of the system to produce voltage and current harmonics. In addition, all control loops that synthetize only fundamental components have THD values below the 3% mark and close to the values presented in fundamental test.

The last test synthetizes harmonic voltage and current simultaneously. Fig. 21 presents the results of the VRC voltage loop control and the CRC current loop control for voltage

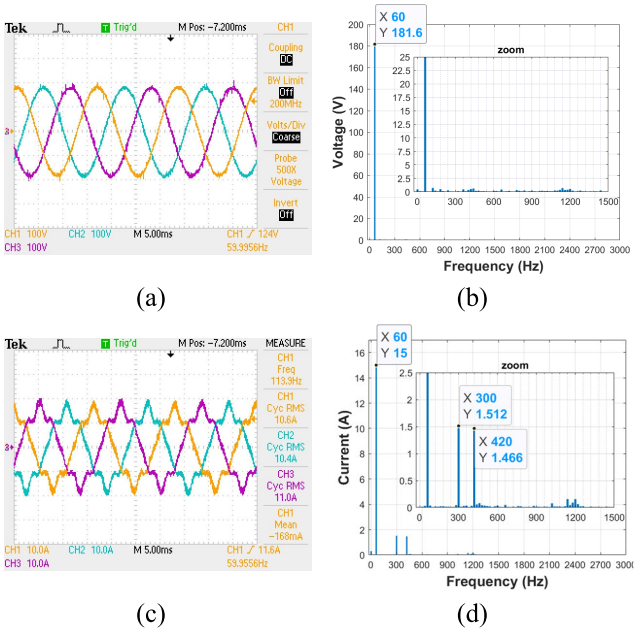

FIGURE 20. Measured current harmonic test results. (a) Three-phase test voltage, (b) Frequency spectrum of the voltage test, (c) Three-phase test current, (d) Frequency spectrum of the current test.

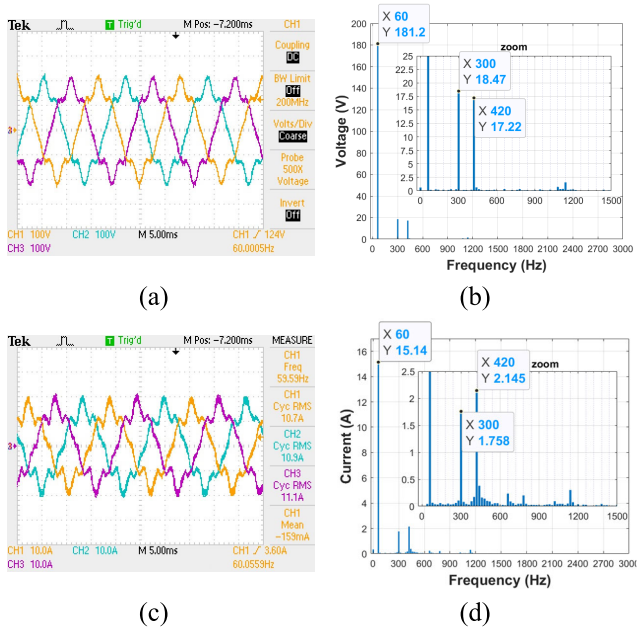

FIGURE 22. Measured full harmonic test results. (a) Three-phase test voltage, (b) Frequency spectrum of the voltage test, (c) Three-phase test current, (d) Frequency spectrum of the current test.

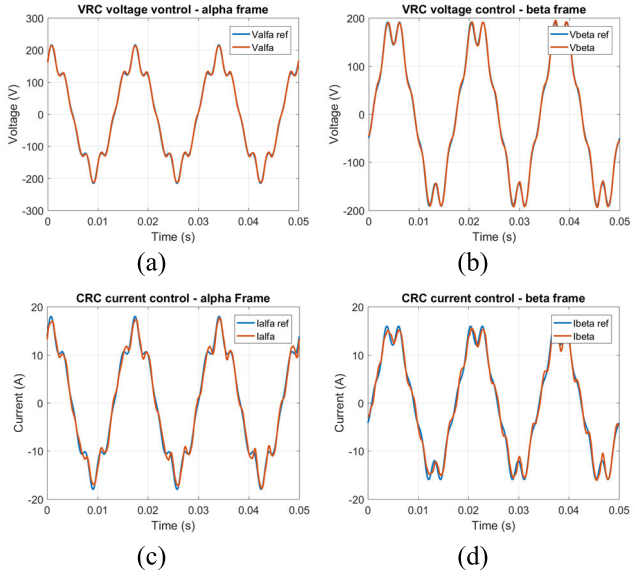

FIGURE 21. VRC and CRC voltage and current control loop reference tracking in full harmonic test. Voltage in (a) alpha frame and (b) beta frame, Current in (c) alpha frame and (d) beta frame.

and current harmonic operation. For the voltage control, error values of 2.35% and 2.57% were registered for the alpha and beta frames, respectively. As for the current control, the values were of 7.10% for the alpha and 8.10% for the beta frame. The voltage errors to reference tracking are higher than the previous ones, although they are still lesser than 3%. However, the current tracking errors is much higher and clearly noticed in the curves. The controller's disturbance rejection is not as good in this case as it was in the previous harmonic tests.

TABLE 8. Voltage and current harmonic distortions in the full harmonic test.

	Voltage	Current
THD	14.05%	18.97%
IHD 5^{th}	10.19%	11.61%
IHD 7^{th}	9.50%	14.16%

Fig. 22 presents the test voltage and current waveforms and their frequency spectrums, and Table 8 shows the voltage and current THD and IHD for this test. These results confirm that the synthetized voltage is close to the reference, but the current presents an error. Through the inspection of the current IHD values, one can see that the 7th harmonic component is the one responsible for the majority of the error. Higher controller gains should lead to better stiffness, although with diminished phase margin and, thus compromising system stability.

Albeit the higher error presented in the harmonic test with simultaneous current and voltage distortions, the experimental results demonstrate the proposed AEL flexibility and capability of controlling both current and voltage in the equipment under test. The test of harmonic distortion on power transformers, although seldom done, is very important, thus, this AEL is an important tool in this sense.

IV. CONCLUSION

This paper presented an AEL capable to perform power transformers test. Its configuration and working principle were explained, and the control system considerations and design

were presented. The influence of each converter in the other was simplified to allow using an individual control design strategy with a simple classical approach. As seen in the results, this simplification did not affect the system stability, but can influence the perturbation rejection capability.

The fundamental frequency tests demonstrated the capability of the test bench to impose current, voltage and frequency to the power transformer with low error. In the harmonic tests, the system flexibility to impose controlled voltage and current distortions were also demonstrated, allowing transformer testing under nonlinear loading conditions. The possibility of independently controlling current and voltage harmonics is a differential of the proposed structure.

Overall, the proposed structure is capable of performing a power transformer test with full control of its electric quantities due to it being decoupled from the electrical grid. Its higher degree of freedom of control is, thus, extremely beneficial and it differentiates this new topology from others reported in the literature.

REFERENCES

[1] IEA. *World Energy Outlook 2020—Analysis—IEA*. Accessed: Mar. 27, 2021. [Online]. Available: https://www.iea.org/reports/world-energy-outlook-2020

[2] T. Jin and J. Kim, "A comparative study of energy and carbon efficiency for emerging countries using panel stochastic frontier analysis," *Sci. Rep.*, vol. 9, no. 1, p. 6647, Dec. 2019, doi: 10.1038/s41598-019-43178-7.

[3] X. Shi, H. Yang, Z. Xu, X. Zhang, and M. R. Farahani, "An independent component analysis classification for complex power quality disturbances with sparse auto encoder features," *IEEE Access*, vol. 7, pp. 20961–20966, 2019, doi: 10.1109/ACCESS.2019.2898211.

[4] J. A. Heerdt, D. F. Coutinho, S. A. Mussa, and M. L. Heldwein, "Control strategy for current harmonic programmed AC active electronic power loads," *IEEE Trans. Ind. Electron.*, vol. 61, no. 8, pp. 3810–3822, Aug. 2014, doi: 10.1109/TIE.2013.2284144.

[5] S.-J. Huang and F.-S. Pai, "Design and operation of burn-in test system for three-phase uninterruptible power supplies," *IEEE Trans. Ind. Electron.*, vol. 49, no. 1, pp. 256–263, Feb. 2002, doi: 10.1109/41.982270.

[6] N. Chen and H. S.-H. Chung, "Energy-recyclable burn-in technology for electronic ballasts," *IEEE Trans. Power Electron.*, vol. 26, no. 9, pp. 2550–2562, Sep. 2011, doi: 10.1109/TPEL.2011.2111386.

[7] Y. Zhao, W. Dong, X. Zou, L. Tong, and G. Zhu, "Analysis and design of power hardware-in-the-loop testing for 400-Hz inverters," in *Proc. 12th IEEE Conf. Ind. Electron. Appl. (ICIEA)*, Siem Reap, Cambodia, Jun. 2017, pp. 1122–1126, doi: 10.1109/ICIEA.2017.8283008.

[8] D. J. Hogan, F. J. Gonzalez-Espin, J. G. Hayes, G. Lightbody, and R. Foley, "An adaptive digital-control scheme for improved active power filtering under distorted grid conditions," *IEEE Trans. Ind. Electron.*, vol. 65, no. 2, pp. 988–999, Feb. 2018, doi: 10.1109/TIE.2017.2726992.

[9] A. F. Cupertino, H. A. Pereira, and V. F. Mendes, "Modeling, design and control of a solar array simulator based on two-stage converters," *J. Control, Automat. Electr. Syst.*, vol. 28, no. 5, pp. 585–596, Oct. 2017, doi: 10.1007/s40313-017-0333-z.

[10] S. P. Freitas, N. A. C. Fernandes, V. F. Mendes, A. F. Cupertino, and H. A. Pereira, "An improved solar array simulator topology based on LCL filter," in *Proc. IEEE 8th Int. Symp. Power Electron. for Distrib. Gener. Syst. (PEDG)*, Florianopolis, Brazil, Apr. 2017, pp. 1–7, doi: 10.1109/PEDG.2017.7972545.

[11] A. Mengatto, F. J. Zimman, and J. A. Heerdt, "High current harmonic control strategy for a T-NPC interleaved AC active electronic power loads," in *Proc. IEEE 13th Brazilian Power Electron. Conf. 1st Southern Power Electron. Conf. (COBEP/SPEC)*, Fortaleza, Brazil, Nov. 2015, pp. 1–6, doi: 10.1109/COBEP.2015.7420209.

[12] Z. Geng, D. Gu, T. Hong, and D. Czarkowski, "Programmable electronic AC load based on a hybrid multilevel voltage source inverter," *IEEE Trans. Ind. Appl.*, vol. 54, no. 5, pp. 5512–5522, Sep./Oct. 2018, doi: 10.1109/TIA.2018.2818059.

[13] T. Galvão and D. Simonetti, "A low-power setup proposal for power transformer loading tests," *Energies*, vol. 12, no. 21, p. 4133, Oct. 2019, doi: 10.3390/en12214133.

[14] B.-M. Han, B.-Y. Bae, and Y.-S. Jeong, "Load simulator with power recovery capability based on voltage source converter–inverter set," *IEE Proc., Electr. Power Appl.*, vol. 153, no. 6, p. 891, 2006, doi: 10.1049/ip-epa:20050461.

[15] W. McDermid and J. Lambert, "Power transformer testing at manitoba Hydro's high voltage test facility," in *Proc. Int. Conf. High Voltage Eng. Appl.*, Shanghai, China, Sep. 2012, pp. 92–94, doi: 10.1109/ICHVE.2012.6357061.

[16] *IEEE Standard Test Code for Liquid-Immersed Distribution, Power, and Regulating Transformers Corrigendum 1:Editorial and Technical Corrections*, IEEE Standard C57.12.90-2015Cor 1-2017 Corrigendum IEEE Standard C57.12.90-2015, Apr. 2017, pp. 1–13.

[17] L. W. Pierce, "An investigation of the temperature distribution in cast-resin transformer windings," *IEEE Trans. Power Del.*, vol. 7, no. 2, pp. 920–926, Apr. 1992, doi: 10.1109/61.127099.

[18] C. V. de Sousa, G. M. de Rezende, F. F. Matos, S. R. Silva, and V. F. Mendes, "Regenerative active electronic load for testing power transformers under linear and nonlinear conditions," *J. Control, Autom. Electr. Syst.*, vol. 27, no. 1, pp. 105–117, Feb. 2016, doi: 10.1007/s40313-015-0220-4.

[19] M. Bajaj and A. K. Singh, "Power quality challenges associated with distributed generation planning: A simulation-based demonstration," in *Proc. Int. Conf. Electr., Electron. Comput. Eng. (UPCON)*, Nov. 2019, pp. 1–6, doi: 10.1109/UPCON47278.2019.8980032.

[20] A. V. Shalukho, I. A. Lipuzhin, and A. A. Voroshilov, "Power quality in microgrids with distributed generation," in *Proc. Int. Ural Conf. Electr. Power Eng. (UralCon)*, Oct. 2019, pp. 54–58, doi: 10.1109/URALCON.2019.8877619.

[21] F. F. Matos, C. V. de Sousa, G. M. de Rezende, R. Toledo, S. I. Seleme, Jr., and E. S. R. Silva, "Projeto e construçao de filtro LCL para conversores PWM," in *Proc. XVIII Congresso Brasileiro de Automática*, Bonito, Brasil, Sep. 2010, pp. 1568–1575.

[22] M. Liserre, F. Blaabjerg, and S. Hansen, "Design and control of an LCL-filter-based three-phase active rectifier," *IEEE Trans. Ind. Appl.*, vol. 41, no. 5, pp. 1281–1291, Sep. 2005, doi: 10.1109/TIA.2005.853373.

[23] M. Liserre, F. Blaabjerg, and S. Hansen, "Design and control of an LCL-filter based three-phase active rectifier," in *Proc. Conf. Rec. IEEE Ind. Appl. Conf. 36th IAS Annu. Meeting*, vol. 1, Oct. 2001, pp. 299–307, doi: 10.1109/IAS.2001.955428.

[24] L. S. Xavier, A. F. Cupertino, V. F. Mendes, and H. A. Pereira, "A novel adaptive current harmonic control strategy applied in multifunctional single-phase solar inverters," in *Proc. IEEE 13th Brazilian Power Electron. Conf. 1st Southern Power Electron. Conf. (COBEP/SPEC)*, Fortaleza, Brazil, Nov. 2015, pp. 1–6, doi: 10.1109/COBEP.2015.7420040.

[25] A. Vidal, F. D. Freijedo, A. G. Yepes, P. Fernandez-Comesana, J. Malvar, Ó. Lopez, and J. Doval-Gandoy, "Assessment and optimization of the transient response of proportional-resonant current controllers for distributed power generation systems," *IEEE Trans. Ind. Electron.*, vol. 60, no. 4, pp. 1367–1383, Apr. 2013, doi: 10.1109/TIE.2012.2188257.

[26] R. Cárdenas, M. Díaz, F. Rojas, J. Clare, and P. Wheeler, "Resonant control system for low-voltage ride-through in wind energy conversion systems," *IET Power Electron.*, vol. 9, no. 6, pp. 1297–1305, May 2016, doi: 10.1049/iet-pel.2015.0488.

[27] A. G. Yepes, F. D. Freijedo, J. Doval-Gandoy, Ó. López, J. Malvar, and P. Fernandez-Comesaña, "Effects of discretization methods on the performance of resonant controllers," *IEEE Trans. Power Electron.*, vol. 25, no. 7, pp. 1692–1712, Jul. 2010, doi: 10.1109/TPEL.2010.2041256.

[28] F. D. Freijedo, E. Rodriguez-Diaz, M. S. Golsorkhi, J. C. Vasquez, and J. M. Guerrero, "A root-locus design methodology derived from the impedance/admittance stability formulation and its application for LCL grid-connected converters in wind turbines," *IEEE Trans. Power Electron.*, vol. 32, no. 10, pp. 8218–8228, Oct. 2017, doi: 10.1109/TPEL.2016.2645862.

[29] D. Perez-Estevez, J. Doval-Gandoy, A. G. Yepes, O. Lopez, and F. Baneira, "Enhanced resonant current controller for grid-connected converters with LCL filter," *IEEE Trans. Power Electron.*, vol. 33, no. 5, pp. 3765–3778, May 2018, doi: 10.1109/TPEL.2017.2770218.

[30] A. Vidal, F. D. Freijedo, A. G. Yepes, J. Malvar, Ó. López, and J. Doval-Gandoy, "Transient response evaluation of stationary-frame resonant current controllers for grid-connected applications," *IET Power Electron.*, vol. 7, no. 7, pp. 1714–1724, Jul. 2014, doi: 10.1049/iet-pel.2013.0597.

[31] K. Ogata, *Modern Control Engineering*, 5th ed. Boston, MA, USA: Prentice-Hall, 2010.
[32] M. Liserre, R. Teodorescu, and F. Blaabjerg, "Stability of photovoltaic and wind turbine grid-connected inverters for a large set of grid impedance values," *IEEE Trans. Power Electron.*, vol. 21, no. 1, pp. 263–272, Jan. 2006, doi: 10.1109/TPEL.2005.861185.

GUILHERME MONTEIRO DE REZENDE received the B.Sc. and M.Sc. degrees in electrical engineering from the Federal University of Minas Gerais (UFMG), Belo Horizonte, Brazil, in 2010 and 2013, respectively, where he is currently pursuing the Ph.D. degree in electrical engineering.

He is currently an Assistant Professor with the Institute of Technological Sciences (ICT), Federal University of Itajubá (UNIFEI), Itabira Campus, Itabira, Brazil. His research interests include the applications of power electronics devices in power quality problems solutions and wind power generation control strategies for low-voltage ride through.

MATHEUS VIEIRA DE ALMEIDA is currently pursuing the bachelor's degree in electrical engineering with the Federal University of Minas Gerais (UFMG), Belo Horizonte, Brazil.

He is currently an Intern with Vallourec Smart Tubular Solutions, working on the electromagnetic design of equipment for non-destructive tests with the company's engineering sector. His research interests include applications in power electronics, electronic design, and electromagnetic analysis.

TIAGO DE SÁ FERREIRA (Member, IEEE) received the B.Sc. and M.Sc. degrees in electrical engineering from the Federal University of Minas Gerais (UFMG), Belo Horizonte, Brazil, in 2011 and 2013, respectively, where he is currently pursuing the Ph.D. degree in electrical engineering.

He is currently an Assistant Professor with the Institute of Technological Sciences (ICT), Federal University of Itajubá (UNIFEI), Itabira Campus, Itabira, Brazil. His research interests include the applications of power electronics solutions to power quality problems, PWM techniques, electronic ballasts, and LED drives.

CLODUALDO VENICIO DE SOUSA received the B.Sc. degree in electrical engineering from the Centro Universitário do Leste de Minas Gerais (UNILESTE), Ipatinga, Brazil, in 2001, and the M.Sc. and Ph.D. degrees in electrical engineering from the Federal University of Minas Gerais (UFMG), Belo Horizonte, Brazil, in 2007 and 2011, respectively.

He is currently a Professor with the Institute of Technological Sciences (ICT), Federal University of Itajubá (UNIFEI), Itabira Campus, Itabira, Brazil. His research interests include electrical drives, wind and solar generation and control, smart grids, and distributed generation.

VICTOR FLORES MENDES (Member, IEEE) received the B.E.E. degree in control and automation engineering and the M.E.E. and Ph.D. degrees in electrical engineering from the Federal University of Minas Gerais (UFMG), Belo Horizonte, Brazil, in 2008, 2009, and 2013, respectively.

In 2010, he developed part of his thesis at the Dresden University of Technology, Dresden, Germany. In 2020, he was a Postdoctoral Researcher with the LAPLACE Laboratory, Toulouse, France. He is currently a Professor with UFMG. His main research interests include wind and photovoltaic energy conversion systems, applications and control of power electronics, and power quality aspects of distributed generation grid integration.